HHS Public Access

Author manuscript

Nat Chem Biol. Author manuscript; available in PMC 2019 February 17.

Published in final edited form as:

Nat Chem Biol. 2018 September ; 14(9): 887–894. doi:10.1038/s41589-018-0114-4.

ykkC riboswitches employ an add-on helix to adjust specificity for polyanionic ligands

Alla Peselis and **Alexander Serganov***

Department of Biochemistry and Molecular Pharmacology, New York University School of Medicine, New York, NY, USA

Abstract

The *ykkC* family of bacterial riboswitches combines several widespread classes that have similar secondary structures and consensus motifs but control different genes in response to different cellular metabolites. Here we report the crystal structures of two distinct *ykkC* riboswitches specifically bound to their cognate ligands ppGpp, a second messenger involved in stress response, or PRPP, a precursor in purine biosynthesis. Both RNAs adopt similar structures and contain a conserved core previously observed in the guanidine-specific *ykkC* riboswitch. However, ppGpp and PRPP riboswitches uniquely employ an additional helical element that joins the ends of the ligand-sensing domains and creates a tunnel for direct and Mg^{2+}-mediated binding of ligands. Mutational and footprinting experiments highlight the importance of conserved nucleotides forming the tunnel and long-distance contacts for ligand binding and genetic response. Our work provides new insights into the specificity of riboswitches and gives a unique opportunity for future studies of RNA evolution.

Evolutionarily conserved non-coding RNA elements termed riboswitches have emerged as one of the most significant means for modulating gene expression in bacteria[1,2]. Previous studies identified and characterized over 20 classes of riboswitches with more riboswitches still awaiting identification of their ligands[3,4]. The cognate ligand for the orphan riboswitch upstream of the *ykkC* gene remained elusive for over a decade[5] until the RNA motif had been recognized as a family of at least 5 subtypes of riboswitches that have very similar consensus sequences and appear to form similar secondary and tertiary structures[6,7]. Nevertheless, subtle sequence differences and additional nucleotides flanking the common

*Correspondence and requests for materials should be addressed to A.S., alexander.serganov@nyumc.org.

Author contributions

A.P. crystallized the riboswitches, determined their structures and conducted biochemical experiments. A.S. contributed to determination and refinement of the structures. A.P. and A.S. wrote the manuscript.

Competing financial interests

The authors declare no competing financial interests.

Reporting Summary. Further information on experimental design is available in the Nature Research Reporting Summary linked to this article.

Data availability. Coordinates for the PRPP riboswitch structures from *Syntrophothermus lipocalidus* have been deposited to the Protein Data Bank with PDB ID codes 6DLT (native), 6DLR (iridium hexamine soak), 6DLQ (Mn^{2+} soak), 6DLS (Tl^{+} soak) and 6DNR (apo structure). Coordinates for ppGpp riboswitch from *Sulfobacillus acidophilus* have been deposited with PDB ID codes 6DMC (native), 6DMD (Mn^{2+} soak), and 6DME (Tl^{+} soak). Other data are available from the authors upon request.

core dramatically affect specificity of *ykkC* riboswitches. Three classes of *ykkC* riboswitches have been shown to respond to three chemically distinct ligands (Supplementary Fig. 1a). The first class (subtype 1 or guanidine-I riboswitch) recognizes guanidine, a small product of protein metabolism that exists in cells as the guanidinium cation[8]. The second (subtype 2a) and third (subtype 2b) classes bind to polyanionic molecules guanosine tetraphosphate (ppGpp; guanosine-3′,5′-bisdiphosphate) and phosphoribosyl pyrophosphate (PRPP; 5-phospho-α-D-ribose 1-diphosphate)[6,7]. PRPP contains a ribose attached to diphosphate and monophosphate moieties through the O1′ and O5′ oxygen atoms of the sugar, respectively. ppGpp consists of a guanosine linked to two diphosphate moieties through the O3′ and O5′ oxygen atoms of the ribose.

The small molecules that each of the three *ykkC* riboswitch subtypes bind dictate the control over different sets of downstream genes. The guanidine-I riboswitch provides feedback regulation of proteins that modify or transport guanidine out of the cells[8]. PRPP is an intermediate during purine biosynthesis[9] and PRPP riboswitches typically modulate expression of genes associated with production of purines[6]. Many PRPP sensors occur in tandem arrangement with a guanine sensor and share a single expression platform[10], thereby uniquely constituting a Boolean IMPLY molecular logic gate made of RNA[6]. The tandem guanine-PRPP arrangement turns gene transcription on when neither ligand is present or when PRPP is bound by the RNA. Gene expression is turned off when the abundance of guanine exceeds that of PRPP. ppGpp is a well-known alarmone produced during various stresses including stringent response, which is caused by a shortage of amino acids[11]. ppGpp acts on many levels and affects replication, transcription, and translation[12]. ppGpp riboswitches control genes involved in biosynthesis and transport of branched-chain amino acids and genes encoding for glutamate synthase and ABC transporters[7]. ppGpp riboswitches often occur near T-boxes and constitute a two-input AND logic gate that is activated under nutrient starvation by the simultaneous presence of uncharged tRNA and ppGpp.

While riboswitches that adopt similar structures but recognize different ligands have been long known, these riboswitches accommodated chemically similar ligands by slightly adjusting the ligand binding pocket[4] and therefore cannot explain how presumably similar *ykkC* riboswitches bind to chemically distinct small molecules. The issue of PRPP and ppGpp recognition is further complicated by the necessity to bind to a larger number of the negatively charged phosphates, unfavourable for RNA binding, together with a smaller number of other chemical moieties than in previously studied phosphate-bearing riboswitch ligands. Available crystal structures of the guanidine-I riboswitch do not suggest how ppGpp and PRPP can be recognized and distinguished from guanidinium cations[13,14].

To understand the molecular basis for ppGpp and PRPP binding and specificity, we have determined the crystal structures of ppGpp and PRPP riboswitches bound to their cognate ligands. Our structural and biochemical results revealed an unprecedented manner for expanding the repertoire of ligand specificities by similar RNA motifs and pose a question on how such similar RNAs have evolved to bind so different ligands.

Results

ykkC riboswitches share a conserved structural core

Consensus sequences for the PRPP and ppGpp riboswitches[6,7] are highly similar and mostly differ by the degree of evolutionary conservation in some positions and by the presence of a conserved guanosine (Supplementary Fig. 1b,c) in the internal loop of helix P3 in the PRPP riboswitch. This guanosine was suggested to form a long-distance pair with a cytosine from the P2-P3 linker in the PRPP riboswitch and be replaced by the nucleobase of ppGpp in the ppGpp riboswitch[7]. We validated several putative PRPP and ppGpp riboswitches by binding assays using Isothermal Titration Calorimetry (ITC) and succeeded in crystallizing *Syntrophothermus lipocalidus* PRPP and *Sulfobacillus acidophilus* ppGpp riboswitches bound to their cognate ligands. The PRPP riboswitch structure at 2.6 Å resolution was determined by heavy-atom phasing and the ppGpp riboswitch structure was solved by molecular replacement at 2.2 Å resolution using the PRPP riboswitch structure as a model (Supplementary Table 1 and Table 2).

Both riboswitches adopt a similar fold that consists of two helical stacks connected by a four-way junction at a small angle and anchored by a long-distance tertiary contact above the junctional region (Fig. 1a-e). Although the overall RNA fold conforms well to the secondary structure consensus (Supplementary Fig. 1b,c), the structures revealed a new helix previously not predicted by bioinformatics (Fig. 1a,b). This helix, designated P1, joins the conserved 5′ and 3′ ends of the riboswitch domain. Other paired regions were renumbered accordingly in the revised secondary structure consensuses (Supplementary Fig. 1d-g).

PRPP, ppGpp, and guanidine-I riboswitch structures demonstrate a striking resemblance (Fig. 1e,f). The three-way junctional fold of the guanidine-I riboswitch[13,14] can be fit well into the structures of PRPP and ppGpp riboswitches and can be considered as a “core” for the *ykkC* riboswitch family. The PRPP and ppGpp riboswitches expand this core by adding the P1 helix that stacks coaxially under P4 and, together with P4 and junctional regions, creates a tunnel for PRPP and ppGpp binding (Fig. 1e).

Despite high similarity in other regions, the 5′ strand at the bottom of P3 in the guanidine-I RNA is moved ~8 Å towards the P1-P2 stem, thereby narrowing the helix and creating a tight binding site for guanidine (Fig. 1f). This site is located above the binding sites for PRPP and ppGpp and does not overlap with them.

Long-range pairing and extra helix specify ligand binding

Addition of P1 converts the three-way junction observed in the guanidine-I riboswitch into a four-way junction and creates new features in both PRPP and ppGpp riboswitches (Fig. 2a-d). P1 is positioned under junctional regions J3–4 and J1–2a and is held collinearly with P4 through stacking interactions involving A72 (A69) (PRPP riboswitch numbering throughout with ppGpp numbers in parentheses) and G6 (G5) (Fig. 2a,b). However, continuous intrastrand stacking between P1 and P4 is broken on the flanks of the A101-G102-G103 (A96-A97-G98) segment of J4–1. Instead of intrastrand stacking, A101 (A96) from this segment participates in cross-strand stacking with C75 (C72) from the bottom base pair of

P4 thereby maintaining a pseudocontinuous P1-P4 helix. The interior of this helical stem forms a tunnel for ligand binding.

The four-way junction is stabilized by a triple composed of an evolutionarily conserved G6 (G5), highly conserved A72 (A69) and conserved G103 (G98) (Fig. 2a,b and Supplementary Fig. 2a,b). Guanosines of this G6•G103•A72 triple bind to the phosphates of PRPP; however, the equivalent triple in the ppGpp riboswitch does not bind to ppGpp. To further stabilize the junction, G6 stacks on G94 which bulges from the P4 stem of the PRPP riboswitch (Fig. 2a,c). In turn, G94 is partially stacked on A74 of J3–4 and G48, looped out from the P2b stem that runs in parallel with P4. As suggested earlier[6], G94 makes the long-range base-pairing with the highly conserved C73 that interacts with the sugar edge of G102 and facilitates ligand binding in the PRPP riboswitch (Fig. 2c). The looping-out of G94 is facilitated by two flanking purine-purine base pairs, A93•A79 and G78•G95, which widen the helix and kink the backbone to form a conformation reminiscent of the S-turn motif found in a number of RNAs (Fig. 2a,e). A similar conformation of the RNA strand with a looped-out guanosine, flanked by the non-canonical G•C and G•G base pairs, was also observed in the guanidine-I riboswitch structure (Fig. 2f)[13,14]. In contrast, the ppGpp riboswitch structure does not have a residue analogous to G94 and the bottom half of P4 is folded into a regular helix without bulges (Fig. 2g). Instead of G94, the guanosine base of ppGpp pairs with C70, a C73 counterpart (Fig. 2d). Thus, the junctional regions in the PRPP and ppGpp riboswitches are stabilized by different means, a long-range G-C pairing or an interaction with the riboswitch ligand (Fig. 2h).

Unlike the bottom parts of P4, the top halves of P4 in the PRPP and ppGpp riboswitch structures are very similar to each other as well as to the structure of the guanidine-I riboswitch (Fig. 1c-f). The long-range P2-P4 contacts are formed by a series of practically identical interactions involving a stretch of purines at the apex of P4 bound to the minor grove of the P2b helix, looped-out G89, and backbone interactions mediated by Mg^{2+}-cations Mg2 and Mg3. In the guanidine-I riboswitch[13,14], the strand opposite to the purine stretch has some irregularities but they do not have impact on the region below as evidenced by comparison with the PRPP and ppGpp riboswitch structures.

PRPP and ppGpp binding involve distinct interactions

Both PRPP and ppGpp are encapsulated within the interior tunnel of the P1-P4 helix along its axis (Fig. 2e,g and Supplementary Fig. 2). Unbiased electron density maps[15] show that both ligands bind RNA in extended conformations so that the O5´-linked phosphate of PRPP and the O3´-linked phosphates of the pseudosymmetrical ppGpp are oriented up towards P4 and the other phosphate moieties are oriented down towards P1 (Supplementary Fig. 3).

Both PRPP and ppGpp engage several riboswitch elements through direct and Mg^{2+}-mediated interactions (Fig. 3 and Supplementary Fig. 2). Two nucleotides of P2b, G48 and U49 (G43 and C44), bind the terminal phosphate of the ligands (Supplementary Fig. 2c,f,g). While G48 (G43) uses its Watson-Crick edge for interactions with the oxygen atoms of the phosphate, U49 (C44) binds the RNA through the Mg1 coordination. On the other side, the same phosphate is recognized by C75 and C76 which are involved in the formation of the bottom base pairs of P4 (Fig. 3a and Supplementary Fig. 2c). In the ppGpp riboswitch, C72,

equivalent to C75, also directly interacts with the phosphate, while C73, equivalent to C76, does not do so (Fig. 3b and Supplementary Fig. 2g,h). Instead, three nucleotides of the U75•G91 and G74•U92 base pairs bind to the terminal phosphate of ppGpp through multiple hydrogen bonds mediated by the outer sphere of the Mg^{2+} cation Mg4. Additional interactions to the terminal and O3′-connected phosphates also include the outer sphere of the Mg^{2+} cation Mg5 and nucleotides of the two bottom base pairs of P4.

A striking difference between PRPP and ppGpp riboswitches is recognition of the ribose moiety present in both ligands. The ribose of PRPP is located within hydrogen bonding distance from the Watson-Crick edges of G6, C75 and G102 and the sugar edge of G94 (Figs. 2a, 3a and Supplementary Fig. 2c,d). In contrast, the ribose of ppGpp does not bind RNA at all. Another noticeable difference is observed for the single-stranded A101-G102-G103 (A96-A97-G98) segment of J4–3 that contains bases oriented towards ligands by their Watson-Crick edges. In the PRPP riboswitch, G102 and G103 interact with the ribose and the diphosphate moiety of the ligand, but A101 does not reach the ligand (Fig. 3a and Supplementary Fig. 2d,e). In contrast, in the ppGpp riboswitch, A96, the equivalent of A101, does interact with the RNA while other nucleotides of the segment do not form direct hydrogen bonds with the RNA (Fig. 3b and Supplementary Fig. 2i). In the PRPP riboswitch, the diphosphate moiety is also directly bound by G6 from J1–2 and A5 from P1 (Fig. 3a); however, in the ppGpp riboswitch, the same diphosphate moiety directly binds only one nucleotide, A4 from P1, and interacts with four nucleotides through the inner and outer spheres of the Mg^{2+} cation Mg6 (Fig. 3b and Supplementary Fig. 3j,k).

The most important difference between PRPP and ppGpp is the presence of a nucleobase in ppGpp. As mentioned above, the ppGpp riboswitch RNA uses this feature for ligand recognition and RNA stabilization. The nucleobase of ppGpp sits above the nucleobase of G5 thereby mediating stacking between P1 and P4 and forms a Watson-Crick pair with C70 to stabilize the non-paired region joining P1 and P4 (Figs. 2d and 3b). To bind C70, the guanosine of ppGpp adopts an uncommon *syn* conformation, which occurs in guanosines more often than in other nucleotides[16]. Such a conformation makes the ligand more compact and ensures its fitting in the tunnel. The multiple interactions of ppGpp with the RNA offset the cost of adopting this less favorable conformation.

Metals assist in structure formation and ligand binding

To validate the identity of metal cations and identify additional metal binding sites (Supplementary Fig. 3), we soaked crystals in solutions containing Mn^{2+} and Tl^{+} that mimic Mg^{2+} and K^{+} cations, respectively, but have stronger anomalous signal. The anomalous maps confirmed the Mg^{2+} cations observed in both riboswitch structures and revealed nine more potential Mg^{2+}-binding sites in the PRPP riboswitch structure that complement the three Mg^{2+} cations found in the native structure (Supplementary Figs. 4 and 5). In both riboswitch structures, Mg^{2+} and Mn^{2+} cations are predominantly scattered in the central part (P2a and P2b) and the P1-P4 stack (Supplementary Figs. 4e and 5d). Despite overall similarity between the PRPP and ppGpp riboswitch structures, only a handful of these cations occupy equivalent sites. The ppGpp riboswitch also contains a high occupancy Tl^{+}/K^{+} cation in the interior loop of P2b (Supplementary Fig. 5b).

Comparison of the ligand-bound cations revealed that in addition to Mg1 that is common to both riboswitches, the PRPP riboswitch contains a Mn^{2+}-binding site matching Mg4 of the ppGpp riboswitch. Therefore, two metal cations may directly assist PRPP in the RNA binding, while recognition of ppGpp involves four Mg^{2+} cations. Among these four cations, Mg4 and Mg5 appear to be stronger binders and Mn^{2+} cations do not substitute for them in short soaks (Supplementary Fig. 5a,c,d).

Alternative base pairing defines ligand specificity

ITC measurements showed that the wild type *S. lipocalidus* PRPP and *S. acidophilus* ppGpp riboswitches bind to their respective ligands, PRPP and ppGpp, with 25.5 and 0.5 μM affinity, respectively, and neither bind to other ligands (Fig. 4a,b and Supplementary Fig. 6a). The structures suggested that removing or mutating G94 in the PRPP riboswitch may disrupt the G94-C73 base pair and allow for base-pairing of C73 with the nucleobase of ppGpp. Accordingly with this prediction, the ΔG94 and G94U mutants abolished PRPP binding and converted the PRPP RNA into a weak ppGpp binder (Fig. 4c and Supplementary Fig. 6a).

Importance of conserved nucleotides for PRPP binding

To understand the impact of conserved nucleotides on ligand binding, we mutated several residues of the PRPP riboswitch. Removal of the P1 helix eliminated PRPP binding (Fig. 4c), thereby emphasizing the essential role of this element for ligand recognition. The A5G substitution removes a contact with PRPP and prompts repelling interactions with its bottom phosphate resulting in reduction of PRPP binding to the level that cannot be adequately determined (Supplementary Fig. 6). The G6A and G103A mutations abolished and greatly reduced PRPP binding, respectively, since they disrupt the G6•G103•A72 triple and remove contacts with the ribose and last phosphate of PRPP (Supplementary Fig. 2a). The formation of the G6•A72 base pair in the triple is critical for ligand binding as A72C also eliminates PRPP binding, although A72 does not reach the ligand. Interestingly, the G102A mutation that eliminates hydrogen bonds with the ribose and the phosphate of PRPP does not have an impact on ligand binding (Fig. 4c). These results suggest that the structural integrity of the RNA may be more important for ligand binding than individual contacts of the RNA with PRPP. Lastly, the U49A substitution is predicted to displace Mg1 from the structure (Fig. 3a). This mutation eliminates ligand binding and proves that the top phosphate of PRPP is essential for interactions with the RNA (Supplementary Fig. 6).

Ligand binding stabilizes the P1-P4 stack

To assess global conformational changes in the PRPP RNA upon PRPP binding, we conducted footprinting with ribonuclease V1 that cleaves continuous paired or stacked regions in RNA. The nuclease cleavage largely coincides with major helices of the riboswitch. Addition of PRPP reproducibly increases resistance of nucleotides in P4 to V1 cleavage (Fig. 5a-c). Weaker protecting effects are observed in P3 and P2a, implying that ligand binding stabilizes the junction and makes adjacent regions more resistant to cleavage. The ligand binding also causes weak enhancements of cleavage in the P2b-P2c region possibly as an effect of the helix stabilization induced by strengthening the tertiary P2b-P4 contact. Previous inline probing experiments revealed PRPP-dependent modulation of this

contact. Projection of the V1 footprinting results on the riboswitch structure (Fig. 5d) identified the strongest protections at G77, G78, G98, and A100, the nucleotides located in the PRPP binding site.

To support mutational data and detect possible conformational rearrangements in the mutated RNAs, we conducted V1 cleavage on the mutants of the PRPP riboswitch used for binding affinity measurements (Fig. 5a,b and Supplementary Fig. 7a,b). All mutants showed cleavage patterns and intensities mostly reminiscent of the wild type RNA, with the exception of ΔG94 that displayed reduction of cleavage in the major cleavage areas (Fig. 5a). As anticipated from the ITC experiments, neither mutant except G102A showed strong modulations upon PRPP binding (Fig. 5a,b and Supplementary Fig. 7a,b). The cleavage pattern was also preserved in the ΔP1 mutant (Supplementary Fig. 7a,c), indicating that removal of the P1 helix does not have a deleterious effect on the conformation of the core RNA and constitutes an essential part of the ligand-binding site.

Apo structure reveals flexibility in ligand-biding region

To identify nucleotides that adjust their conformation upon ligand binding, we solved the structure of the PRPP riboswitch in the absence of PRPP (Fig. 6a). This structure is remarkably similar to the ligand-bound state, as was described for several other riboswitch systems[17–20]. A small shift occurred in the A101-G102-G103 segment, suggesting inherent flexibility of this region likely required for ligand binding (Fig. 6b). A second change, which possibly helped to obtain the ligand-free structure, involves G1 and its 5′ triphosphorylated moiety that was pivoted into the ligand-binding tunnel. In the tunnel, the phosphates of the 5′ end mimicked two phosphates of PRPP and partially stabilized helix P1, thereby facilitating crystallization. The PRPP-free structure contains Mg2 and Mg3 cations but not the ligand-bound Mg1 which is likely brought with PRPP (Fig. 6a).

Discussion

Our work provides the first insights into the structural organization and ligand specificity of the PRPP and ppGpp riboswitches from the *ykkC* riboswitch family. These two broadly-spread classes of riboswitches are similar in structure but specifically bind different ligands and do not interact with guanidine, a ligand for another riboswitch class within the same family. Despite sharing a highly similar core structure with guanidine-I riboswitch, PRPP and ppGpp riboswitches form an additional helix that creates a tunnel for specific binding of ppGpp and PRPP. These tunnels contain many common features but are uniquely adjusted for recognition of the cognate ligands using different sets of direct and Mg^{2+}-mediated interactions. Although PRPP and ppGpp share similar chemical moieties, the PRPP riboswitch primarily interacts with PRPP through base-ligand interactions and exploits only a single Mg^{2+} cation for metal-mediated contacts, while the ppGpp riboswitch predominantly makes Mg^{2+}-mediated interactions with ppGpp using four Mg^{2+} cations, unprecedentedly large number of cations for riboswitch ligand binding[21–27].

The most dramatic difference in recognition of PRPP and ppGpp is a substitution of the long-range base pair in the PRPP riboswitch by a ligand-RNA pairing in the ppGpp riboswitch. Disruption of this base pair by a single-nucleotide deletion or substitution

convert the PRPP riboswitch into a ppGpp binder albeit with >100 fold lower affinity compared to the natural ppGpp riboswitch. Possibly, the PRPP riboswitch scaffold may be tuned for low affinity ligand binding by slightly different tertiary P2b-P4 interactions that have potential to affect the overall stability of the RNA. Alternatively, high affinity ppGpp binding may require specific adjustments in the vicinity of the ligand-binding tunnel, such as reduction of the G94 loop to prevent its clashing with the sugar of ppGpp.

The PRPP and ppGpp riboswitch structures revealed several positions that may contribute to ligand specificity. Two purine-purine base pairs which flank G94 disrupt a regular helix and facilitate looping out of G94 required for PRPP binding. While the top A•A base pair is moderately conserved and the bottom base pair could be both canonical and non-canonical in the PRPP riboswitch, in the ppGpp riboswitch, these two base pairs are moderately conserved standard G-Y and G•U base pairs that likely prevent formation of the loop that interferes with ppGpp binding. The specificity to guanidine in the guanidine-I riboswitches[13,14] is possibly defined by highly conserved G•G and G•A base pairs located below the looped out guanosine. These two base pairs break the regular helix observed in the PRPP riboswitch structure and move the 3′ strand inwards to make a narrower binding site for guanidine (Fig. 2f).

The two-layered mechanism of ligand discrimination in the *ykkC* riboswitch family by employing an additional element and adjusting its specificity does not have parallels in other riboswitch systems. All other riboswitches make subtle changes in the ligand-binding pockets to accommodate a variant natural ligand with a similar chemical structure. For example, specificity of adenine and guanine riboswitches is interconverted by changing a single pyrimidine, cytosine or uridine, that base-pairs with the ligand, guanine or adenine, respectively[28–30]. Highly similar to the guanine riboswitch, the deoxy-guanosine riboswitch contains several changes in the ligand binding pocket to accommodate the sugar moiety of the ligand[31–33]. Such small adaptations could be compared to the changes in the ligand-binding tunnels for specific accommodations of PRPP and ppGpp. However, neither riboswitch described earlier[34–38] employed an additional structural element to switch ligand specificity. The guanidine-I riboswitch does not have this add-on element and therefore cannot bind PRPP and ppGpp.

While the PRPP riboswitch is tuned to recognize a ligand without a nucleobase, ppGpp contains a GDP moiety common to many small molecules present in the cell. Therefore, in addition to Watson-Crick base-pairing for nucleobase recognition, the RNA makes many interactions with the O3′ diphosphate moiety of ppGpp and especially with its terminal phosphate, not present in nucleotides and related compounds. At the same time, the riboswitch measures the length of the ligand by binding to the O5′ diphosphate moiety and employs direct coordination to Mg^{2+} cation to its terminal phosphate. Interestingly, there is extra space at the bottom of the ligand-binding tunnel suggesting that the riboswitch may accommodate an additional phosphate of pppGpp, an alarmone related to ppGpp[39].

Our results explain the molecular mechanism of action of the PRPP and ppGpp riboswitches. In the absence of the ligand, both riboswitches can form transcription terminators by base-pairing the 3′ regions of the sensing domains with the downstream

sequences (Fig. 6c and Supplementary Fig. 8) and, similar to riboswitches from other species[6,7], turn off transcription of the gene. Our structural and footprinting data show that the same 3′ regions are involved in the ligand binding and formation of the P1-P4 helix, an element that prevents formation of the terminator and allows transcription to proceed to the end. Our structural data also provide a clue on the mechanism of the IMPLY logic gate of the tandem guanine-PRPP riboswitches[6]. In the tandem riboswitch, the 5′ region of the PRPP sensor overlaps with the 3′ region of the preceding guanine sensor, therefore formation of the ligand-bound guanine and PRPP sensors is mutually exclusive and depends on the availability of guanine and PRPP (Fig. 6d).

Examples of *ykkC* riboswitches with different specificities and similar structures illustrate the high versatility of the RNA, which can adapt to bind chemically different ligands using similar structural solutions[6]. Why the guanidine-I riboswitch scaffold, which is not conceptually different from other junctional riboswitches, is used for evolution of riboswitches with distinct specificities is not clear. In addition, two structurally unrelated RNAs (guanidine-II and –III riboswitches) specifically bind guanidine[40–42]. How distinct guanidine riboswitches and similar *ykkC* riboswitches have emerged during evolution remains a puzzling question for future studies.

METHODS

RNA and complex preparation.

Putative PRPP and ppGpp riboswitches were identified using Infernal 1.1[43,44] and the consensus sequences of the *ykkC* motifs as described previously[45]. Conservation of the nucleotides involved in the putative long-distance G-C base pair was enforced for PRPP riboswitches. The identity of genes under riboswitch control was the deciding factor in selecting riboswitches for biochemical validation. The sensing domains of the *Syntrophothermus lipocalidus* PRPP and *Sulfobacillus acidophilus* ppGpp riboswitches followed by a hammerhead ribozyme were prepared by PCR amplification from the DNA template composed of chemically synthesized oligonucleotides. The PCR fragments were digested by *Hind*III and cloned into the pUT7 vector prepared with *Hind*III and *Stu*I[46].

The RNA constructs designed for crystallization carry several internal mutations, highlighted in Fig. 1, to facilitate crystallization. Specifically, the non-conserved C11-G51 base pair was replaced by the U-A base pair to prevent strand sliding in the helix of the PRPP riboswitch. Additional mutations convert non-conserved apical loops in both the PRPP and ppGpp riboswitches by the GAGA or UUCG tetraloops to create better crystal packing interactions. Both the PRPP and ppGpp riboswitch RNAs contain an extra G at the 5′ end to facilitate transcription by T7 RNA polymerase. The ppGpp construct has a substituted U in the semi-conserved C at the penultimate position on the 3′ end to facilitate cleavage by the hammerhead ribozyme. The crystallization construct of the PRPP riboswitch binds PRPP similar to the wild type RNA (K_d=67.5±10.5 μM, n=2). The plasmids were amplified in the *E.coli* strain DH5α and purified using PureLink HiPure Plasmid Gigaprep Kit (Life Technologies). The plasmids were linearized by *Hind*III at 37 °C overnight and purified by phenol-chloroform extraction. The plasmids were then precipitated by ethanol and dissolved in water. The plasmid DNAs were used as templates for preparative *in vitro*

T7 RNA polymerase transcription[46]. Transcription reactions were conducted in a 30 ml mixture of 0.1 M Tris-HCl buffer, pH 7.9, 30 mM DTT, 12 mM $MgCl_2$, 2 mM spermidine, 2 mM of each ribonucleotide triphosphates, 50 μg/ml DNA template, and 0.06 mg/ml RNA polymerase. Transcription reactions were typically incubated for 4 h at 37 °C and after adjusting $MgCl_2$ to 20 mM incubation continued for 45 min to complete the ribozyme cleavage. Transcription mixtures were frozen, thawed, and centrifuged at 15,000 g for 30 min to remove precipitate. RNA was then purified by denaturing polyacrylamide gel electrophoresis followed by electroelution and ethanol precipitation. To remove remaining contaminants, RNA was further purified by anion-exchange chromatography on a DEAE column (GE Healthcare) and precipitated by ethanol.

PRPP (purity ≥75%), ppGpp (purity ≥85%) and guanidine (purity ≥99%) were purchased from Santa Cruz Biotechnology, TriLink Biotechnology, and Sigma, respectively. Compounds were dissolved in water at concentrations of 100 (ppGpp) and 200 mM (PRPP and guanidine) and stored in aliquots at −20 °C. Riboswitch complexes were prepared by mixing 0.5 mM RNA and 1.5 mM ligands in a buffer containing 20 mM Tris-HCl, pH 6.8 (or 20 mM Tris-HCl pH 7.0 for ppGpp), 50 mM KCl, and 5 mM $MgCl_2$. The complexes were heated at 42 °C for 10 min, and cooled at room temperature prior to crystallization.

Crystallization and structure determination.

Riboswitch crystals were grown by hanging-drop vapor diffusion after mixing 0.5 μl complex with 0.5 μl reservoir solution at 18 °C. The reservoir solution for the ligand-bound and *apo* PRPP riboswitch contained 0.2 M NH_4-acetate, 0.1 M HEPES-KOH pH 7.4, and 45% 2-methyl-2,4-pentanediol (v/v). The solution for the ppGpp riboswitch contained 0.075 M $MgCl_2$, 0.1 M Na-acetate pH 4.2, and 21% PEG400 (v/v). The same crystallization conditions yielded two crystal forms with $C2$ and $P2_1$ space groups. For heavy atom soaking, riboswitch crystal drops were given 0.2 μL of 3 mM heavy atom in mother liquor, and soaked for 4 h. For data collection, crystals were picked and flash-frozen in liquid nitrogen. X-ray diffraction data were collected at 100 K at the (i) 17-ID-2 beamline (Brookhaven National Laboratory): $MnCl_2$ and Tl-acetate soaks of both riboswitch crystals; (ii) 24-ID-C (Argonne National Laboratory): $[Ir(NH_3)_6]^{3+}$ soak of the PRPP riboswitch crystals; and (iii) 24-ID-E (Argonne National Laboratory) for all other crystals. The data were collected at 1.105 Å (PRPP Ir; ppGpp Tl and Mn), 0.9792 Å (PRPP native, Mn and apo; ppGpp native) and 0.9795 Å (PRPP Tl) wave length. The data were reduced using HKL2000 (HKL Research) (Supplementary Table 1 and Table 2). The resolution limits were determined based on several criteria, including $CC_{1/2} > 0.5$[47] and $I/\sigma I > 1.0$ in the high-resolution shell. The PRPP structure was phased by single anomalous diffraction (SAD) using iridium hexamine-soaked crystals of the PRPP riboswitch and PHENIX AutoSol routine[15]. The RNA was partially traced using PHENIX Autobuild routine[48]. Tracing was completed manually in Coot[49] and the structure was refined by PHENIX[50]. The structure of the ppGpp riboswitch was determined by molecular replacement using the iridium hexamine data set in $C2$ space group, predicted to have one RNA molecule in the asymmetric unit. Molecular replacement was conducted in Phaser[51] using the search model composed of the regions that form the central part of the PRPP riboswitch core (nts 2–17, 44–58, 69–74, 81–91, and 102–107). The molecular replacement yielded a single solution with LLG=135.776

and TFZ=7.8. The RNA modeling was complete through iterative rounds of autobuilding, manual building, and simulated annealing refinement, guided by simulated annealing omit electron density maps. All residues of both riboswitch structures were built although residues 57–61 in molecule B ($P2_1$ space group) of the ppGpp riboswitch have less well-defined maps than the rest of the structure. The structures of the ppGpp riboswitch were refined with Refmac[52]. *Apo* and metal-soaked structures were determined by molecular replacement using the corresponding RNA structures as search models. Ligands, metal cations and waters were added at the later stages of refinement. Metal cations were added based on coordination geometry and distances, anomalous signals of related atoms (Mn^{2+} for Mg^{2+}; Tl^{+} for K^{+}), and $2F_o$-F_c and F_o-F_c omit electron density maps. The 2.2 Å electron density map for the native ppGpp structure was of quality sufficient for building water molecules directly coordinated to metal cations. Figures were prepared with PyMol (http://pymol.org/).

Preparation of mutant RNAs.

Mutagenesis was conducted by inverse PCR using oligonucleotides with desired mutations and DNA plasmids bearing wild-type RNA sequences as templates. The PCR mixtures were treated by *Dpn*I to remove DNA template, ligated and transformed into the *E.coli* DH5α. Mutant plasmid DNAs were verified by sequencing. Clones with correct plasmid DNAs were grown in large volume and plasmid DNAs were extracted by the Maxiprep Kit (Qiagen). Mutant RNAs were prepared by *in vitro* transcription and purified by the same procedure as wild type RNAs.

ITC measurements.

Experiments were performed 2–5 times with independently prepared riboswitch samples using the Microcal calorimeter ITC200 at 25 °C. Experiments were conducted with the wild-type PRPP riboswitch RNA or its mutants and the ppGpp riboswitch RNA used for crystallization. Prior to titration, 0.01–0.2 mM RNA samples were dialyzed overnight at 4 °C against experimental buffer containing 50 mM HEPES-KOH, pH 6.8 or 7.9 , 50 mM KCl and 5 or 20 mM $MgCl_2$, for ppGpp or PRPP riboswitches, respectively. The ppGpp samples were heated at 42 °C for 10 min, cooled at room temperature, and centrifuged at 20,000× g at 25 °C for 10 min. The PRPP samples were allowed to warm to room temperature and then centrifuged at 20,000x g at 25 °C for 10 min. For measurements, the PRPP, ppGpp, and guanidine ligands were back-diluted from a high concentration into dialysis buffer to concentrations of 10–30 fold higher than the RNA concentration and were typically titrated into the RNA solution in the sample cell (V=207 μL) by 16–18 serial injections of 2 μL each, with 180 s intervals between injections and a reference power of 10 μcal sec^{-1}. Data were corrected by subtracting heats of the ligand dilution and analyzed by a single-site binding model in Origin 7.0 software (Microcal, Inc). Values were reported as average ± standard error (n=2).

Nuclease Probing and Footprinting

For footprinting experiments, the riboswitch RNAs were radioactively labelled at the 5′ end and purified by 8 M urea/10% polyacrylamide gel electrophoresis (PAGE). 10 μL samples of the radiolabelled RNA (500,000 counts/min) were preheated at 42 °C for 10 min in 50 mM

Tris-HCl pH 7.2, 100 mM KCl, and 5 mM $MgCl_2$. The samples were chilled on ice followed by the addition of 2 mM of the PRPP ligand. The complex was then incubated at 42 °C for 10 min and chilled on ice. Following the formation of the complex, cleavage reactions were performed with 0.72 U RNase V1 (Pierce) at 37 °C for 10 min. Reactions were quenched by the addition of 80 μl cold buffer supplemented with 0.5 μg of tRNA, immediately extracted with phenol-chloroform, and precipitated by ethanol. RNA pellets were dissolved and analyzed by PAGE. Nuclease effects were quantified after normalization and background subtraction by using ImageJ. Experiments were repeated 3 times.

Supplementary Material

Refer to Web version on PubMed Central for supplementary material.

Acknowledgements

We thank D. Fenyo for help with bioinformatics searches. We thank personnel of beamlines 17-ID-2 at the Brookhaven National Laboratory and 24-ID at the Argonne National Laboratory for help with data collection. This research was supported by the NIH grants R01GM112940 to A.S., F31GM119357 and T32 GM88118 to A.P. This work uses the Northeastern Collaborative Access Team beamlines, which are funded by the National Institutes of Health (NIH) grants (P41 GM103403 and S10 RR029205) and resources of the Advanced Photon Source, operated for the DOE Office of Science under Contract No. DE-AC02–06CH11357. The beamline 17-ID-2 is supported in part by the DOE Office of Biological and Environmental Research (KP1605010, KC0401040) and by the NIH (P41GM111244).

References

1. Serganov A, Nudler E A decade of riboswitches. Cell 152, 17–24 (2013). [PubMed: 23332744]
2. Breaker RR Prospects for riboswitch discovery and analysis. Mol Cell 43, 867–79 (2011). [PubMed: 21925376]
3. Greenlee EB et al. Challenges of ligand identification for the second wave of orphan riboswitch candidates. RNA Biol 15, 377–390 (2018). [PubMed: 29135333]
4. McCown PJ, Corbino KA, Stav S, Sherlock ME, Breaker RR Riboswitch diversity and distribution. RNA 23, 995–1011 (2017). [PubMed: 28396576]
5. Barrick JE et al. New RNA motifs suggest an expanded scope for riboswitches in bacterial genetic control. Proc. Natl. Acad. Sci. U S A 101, 6421–6426 (2004). [PubMed: 15096624]
6. Sherlock ME, Sudarsan N, Stav S, Breaker RR Tandem riboswitches form a natural Boolean logic gate to control purine metabolism in bacteria. Elife 7, e33908 (2018). [PubMed: 29504937]
7. Sherlock ME, Sudarsan N, Breaker RR Riboswitches for the alarmone ppGpp expand the collection of RNA-based signaling systems. Proc Natl Acad Sci U S A, doi: 10.1073/pnas.1720406115 (2018).
8. Nelson JW, Atilho RM, Sherlock ME, Stockbridge RB, Breaker RR Metabolism of free guanidine in bacteria is regulated by a widespread riboswitch class. Mol Cell 65, 220–230 (2017). [PubMed: 27989440]
9. Hove-Jensen B et al. Phosphoribosyl Diphosphate (PRPP): biosynthesis, enzymology, utilization, and metabolic significance. Microbiol Mol Biol Rev 81, pii: e00040–16 (2017). [PubMed: 28031352]
10. Sudarsan N et al. Tandem riboswitch architectures exhibit complex gene control functions. Science 314, 300–304 (2006). [PubMed: 17038623]
11. Hauryliuk V, Atkinson GC, Murakami KS, Tenson T, Gerdes K Recent functional insights into the role of (p)ppGpp in bacterial physiology. Nat Rev Microbiol 13, 298–309 (2015). [PubMed: 25853779]
12. Steinchen W, Bange G The magic dance of the alarmones (p)ppGpp. Mol Microbiol 101, 531–44 (2016). [PubMed: 27149325]

13. Reiss CW, Xiong Y, Strobel SA Structural basis for ligand binding to the guanidine-I riboswitch. Structure 25, 195–202 (2017). [PubMed: 28017522]
14. Battaglia RA, Price IR, Ke A Structural basis for guanidine sensing by the ykkC family of riboswitches. RNA 23, 578–585 (2017). [PubMed: 28096518]
15. Adams PD et al. PHENIX: building new software for automated crystallographic structure determination. Acta Crystallogr D Biol Crystallogr 58, 1948–54 (2002). [PubMed: 12393927]
16. Sokoloski JE, Godfrey SA, Dombrowski SE, Bevilacqua PC Prevalence of syn nucleobases in the active sites of functional RNAs. RNA 17, 1775–87 (2011). [PubMed: 21873463]
17. Serganov A, Huang L, Patel DJ Structural insights into amino acid binding and gene control by a lysine riboswitch. Nature 455, 1263–1267 (2008). [PubMed: 18784651]
18. Huang L, Serganov A, Patel DJ Structural insights into ligand recognition by a sensing domain of the cooperative glycine riboswitch. Mol Cell 40, 774–86 (2010). [PubMed: 21145485]
19. Garst AD, Heroux A, Rambo RP, Batey RT Crystal structure of the lysine riboswitch regulatory mRNA element. J Biol Chem 283, 22347–51 (2008). [PubMed: 18593706]
20. Vicens Q, Mondragon E, Batey RT Molecular sensing by the aptamer domain of the FMN riboswitch: a general model for ligand binding by conformational selection. Nucleic Acids Res 39, 8586–98 (2011). [PubMed: 21745821]
21. Serganov A, Polonskaia A, Phan AT, Breaker RR, Patel DJ Structural basis for gene regulation by a thiamine pyrophosphate-sensing riboswitch. Nature 441, 1167–1171 (2006). [PubMed: 16728979]
22. Serganov A, Huang L, Patel DJ Coenzyme recognition and gene regulation by a flavin mononucleotide riboswitch. Nature 458, 233–7 (2009). [PubMed: 19169240]
23. Thore S, Leibundgut M, Ban N Structure of the eukaryotic thiamine pyrophosphate riboswitch with its regulatory ligand. Science 312, 1208–1211 (2006). [PubMed: 16675665]
24. Edwards TE, Ferre-D'Amare AR Crystal structures of the thi-box riboswitch bound to thiamine pyrophosphate analogs reveal adaptive RNA-small molecule recognition. Structure 14, 1459–1468 (2006). [PubMed: 16962976]
25. Klein DJ, Ferre-D'Amare AR Structural basis of glmS ribozyme activation by glucosamine-6-phosphate. Science 313, 1752–1756 (2006). [PubMed: 16990543]
26. Cochrane JC, Lipchock SV, Strobel SA Structural investigation of the GlmS ribozyme bound to its catalytic cofactor. Chem Biol 14, 97–105 (2007). [PubMed: 17196404]
27. Ren A, Patel DJ c-di-AMP binds the ydaO riboswitch in two pseudo-symmetry-related pockets. Nat Chem Biol 10, 780–6 (2014). [PubMed: 25086509]
28. Mandal M, Breaker RR Adenine riboswitches and gene activation by disruption of a transcription terminator. Nat. Struct. Mol. Biol 11, 29–35 (2004). [PubMed: 14718920]
29. Serganov A et al. Structural basis for discriminative regulation of gene expression by adenine- and guanine-sensing mRNAs. Chem Biol 11, 1729–1741 (2004). [PubMed: 15610857]
30. Mandal M, Boese B, Barrick JE, Winkler WC, Breaker RR Riboswitches control fundamental biochemical pathways in Bacillus subtilis and other bacteria. Cell 113, 577–586 (2003). [PubMed: 12787499]
31. Edwards AL, Batey RT A structural basis for the recognition of 2'-deoxyguanosine by the purine riboswitch. J Mol Biol 385, 938–48 (2009). [PubMed: 19007790]
32. Pikovskaya O, Polonskaia A, Patel DJ, Serganov A Structural principles of nucleoside selectivity in a 2'-deoxyguanosine riboswitch. Nat Chem Biol 7, 748–55 (2011). [PubMed: 21841796]
33. Kim JN, Roth A, Breaker RR Guanine riboswitch variants from Mesoplasma florum selectively recognize 2'-deoxyguanosine. Proc Natl Acad Sci U S A 104, 16092–16097 (2007). [PubMed: 17911257]
34. Regulski EE et al. A widespread riboswitch candidate that controls bacterial genes involved in molybdenum cofactor and tungsten cofactor metabolism. Mol. Microbiol 68, 918–932 (2008). [PubMed: 18363797]
35. Nelson JW et al. Control of bacterial exoelectrogenesis by c-AMP-GMP. Proc Natl Acad Sci U S A 112, 5389–94 (2015). [PubMed: 25848023]
36. Ren A et al. Structural basis for molecular discrimination by a 3',3'-cGAMP sensing riboswitch. Cell Rep 11, 1–12 (2015). [PubMed: 25818298]

37. Smith KD, Lipchock SV, Livingston AL, Shanahan CA, Strobel SA Structural and biochemical determinants of ligand binding by the c-di-GMP riboswitch. Biochemistry 49, 7351–9 (2010). [PubMed: 20690679]
38. Kellenberger CA et al. GEMM-I riboswitches from Geobacter sense the bacterial second messenger cyclic AMP-GMP. Proc Natl Acad Sci U S A 112, 5383–8 (2015). [PubMed: 25848022]
39. Liu K, Bittner AN, Wang JD Diversity in (p)ppGpp metabolism and effectors. Curr Opin Microbiol 24, 72–9 (2015). [PubMed: 25636134]
40. Reiss CW, Strobel SA Structural basis for ligand binding to the guanidine-II riboswitch. RNA 23, 1338–1343 (2017). [PubMed: 28600356]
41. Huang L, Wang J, Lilley DMJ The structure of the Guanidine-II riboswitch. Cell Chem Biol 24, 695–702 e2 (2017). [PubMed: 28529131]
42. Huang L, Wang J, Wilson TJ, Lilley DMJ Structure of the Guanidine III riboswitch. Cell Chem Biol 24, 1407–1415 e2 (2017). [PubMed: 28988949]
43. Yao Z et al. A computational pipeline for high- throughput discovery of cis-regulatory noncoding RNA in prokaryotes. PLoS Comput Biol 3, e126 (2007). [PubMed: 17616982]
44. Nawrocki EP, Eddy SR Infernal 1.1: 100-fold faster RNA homology searches. Bioinformatics 29, 2933–5 (2013). [PubMed: 24008419]
45. Barrick JE Predicting riboswitch regulation on a genomic scale. Methods Mol Biol 540, 1–13 (2009). [PubMed: 19381548]
46. Peselis A, Gao A, Serganov A Preparation and crystallization of riboswitches. Methods Mol Biol 1320, 21–36 (2016). [PubMed: 26227035]
47. Karplus PA, Diederichs K Assessing and maximizing data quality in macromolecular crystallography. Curr Opin Struct Biol 34, 60–8 (2015). [PubMed: 26209821]
48. Terwilliger TC et al. Iterative model building, structure refinement and density modification with the PHENIX AutoBuild wizard. Acta Crystallogr D Biol Crystallogr 64, 61–9 (2008). [PubMed: 18094468]
49. Emsley P, Lohkamp B, Scott WG, Cowtan K Features and development of Coot. Acta Crystallogr D Biol Crystallogr 66, 486–501 (2010). [PubMed: 20383002]
50. Afonine PV et al. Towards automated crystallographic structure refinement with phenix.refine. Acta Crystallogr D Biol Crystallogr 68, 352–67 (2012). [PubMed: 22505256]
51. McCoy AJ et al. Phaser crystallographic software. J Appl Crystallogr 40, 658–674 (2007). [PubMed: 19461840]
52. Murshudov GN, Vagin AA, Dodson EJ Refinement of macromolecular structures by the maximum-likelihood method. Acta Crystallogr. D Biol. Crystallogr 53, 240–255 (1997). [PubMed: 15299926]

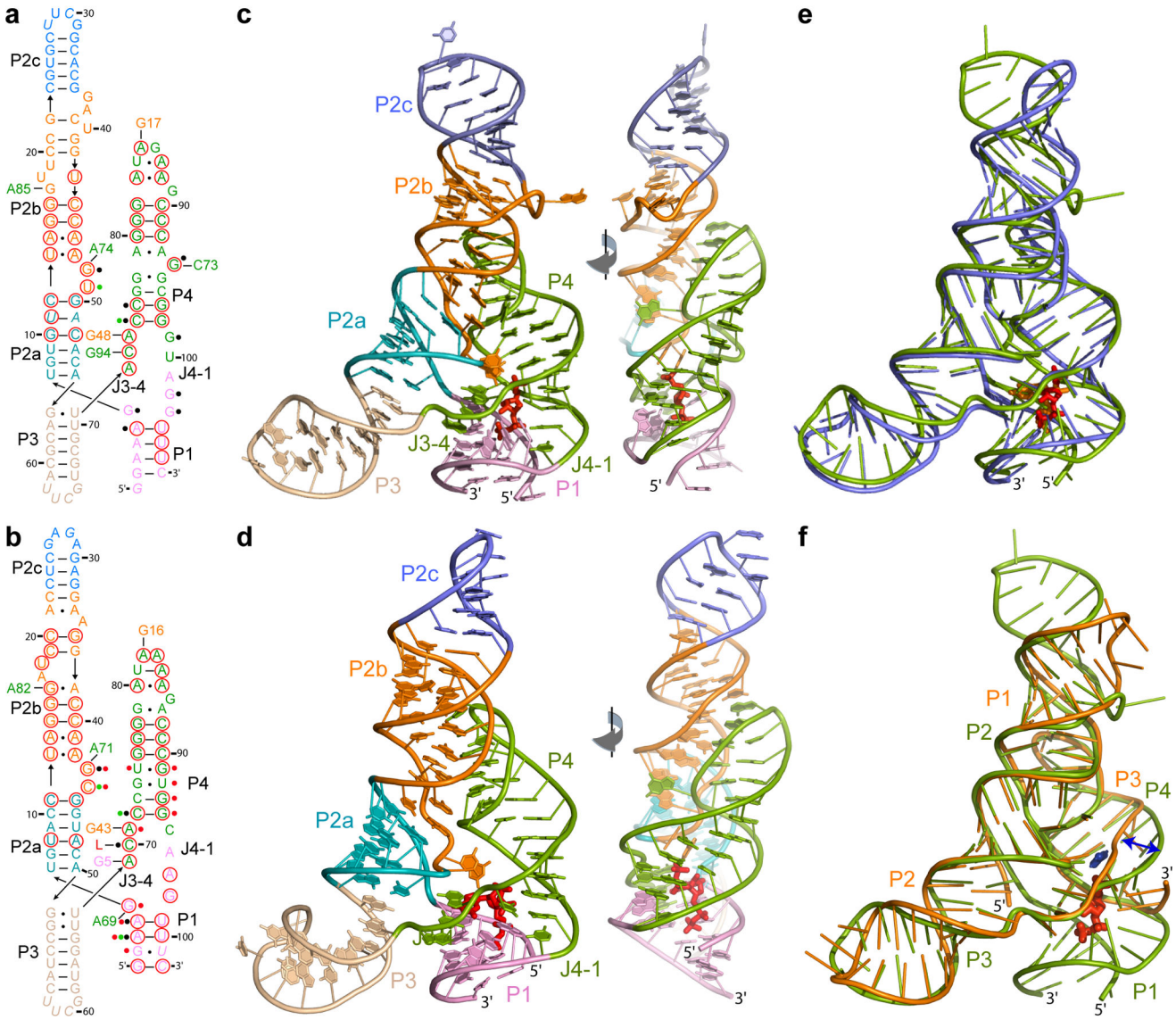

Figure 1.

Overall structures and schematics of the ligand-bound *S. lipocalidus* PRPP and *S. acidophilus* ppGpp riboswitches. (**a**, **b**) Secondary structure schematics of the PRPP (a) and ppGpp (b) riboswitch folds observed in the crystal structure of the complex. Italicized nucleotides altered for crystallization. RNA bases involved in direct, and inner- or outer-sphere Mg^{2+}-coordinated interactions are indicated by black, green and red circles, respectively. Encircled nucleotides are 97% conserved. Watson-Crick and non-canonical base pairs are depicted by lines and black dots, respectively. Partners in the long-range interactions are shown by a line, base and number. L; nucleobase of ppGpp. (**c**, **d**) Front and side views of the PRPP (c) and ppGpp (d) riboswitch structures in cartoon representation. PRPP and ppGpp are shown in red sticks. (**e**) All-atom superposition of the ppGpp (blue) and PRPP (green) riboswitches. ppGpp in orange; PRPP in red. (**f**) Overlay of the PRPP (green) and guanidine-I (orange, PDB ID 5U3G) riboswitch structures. PRPP in red;

guanidine in blue. The double-headed blue arrow shows the conformational difference between two structures.

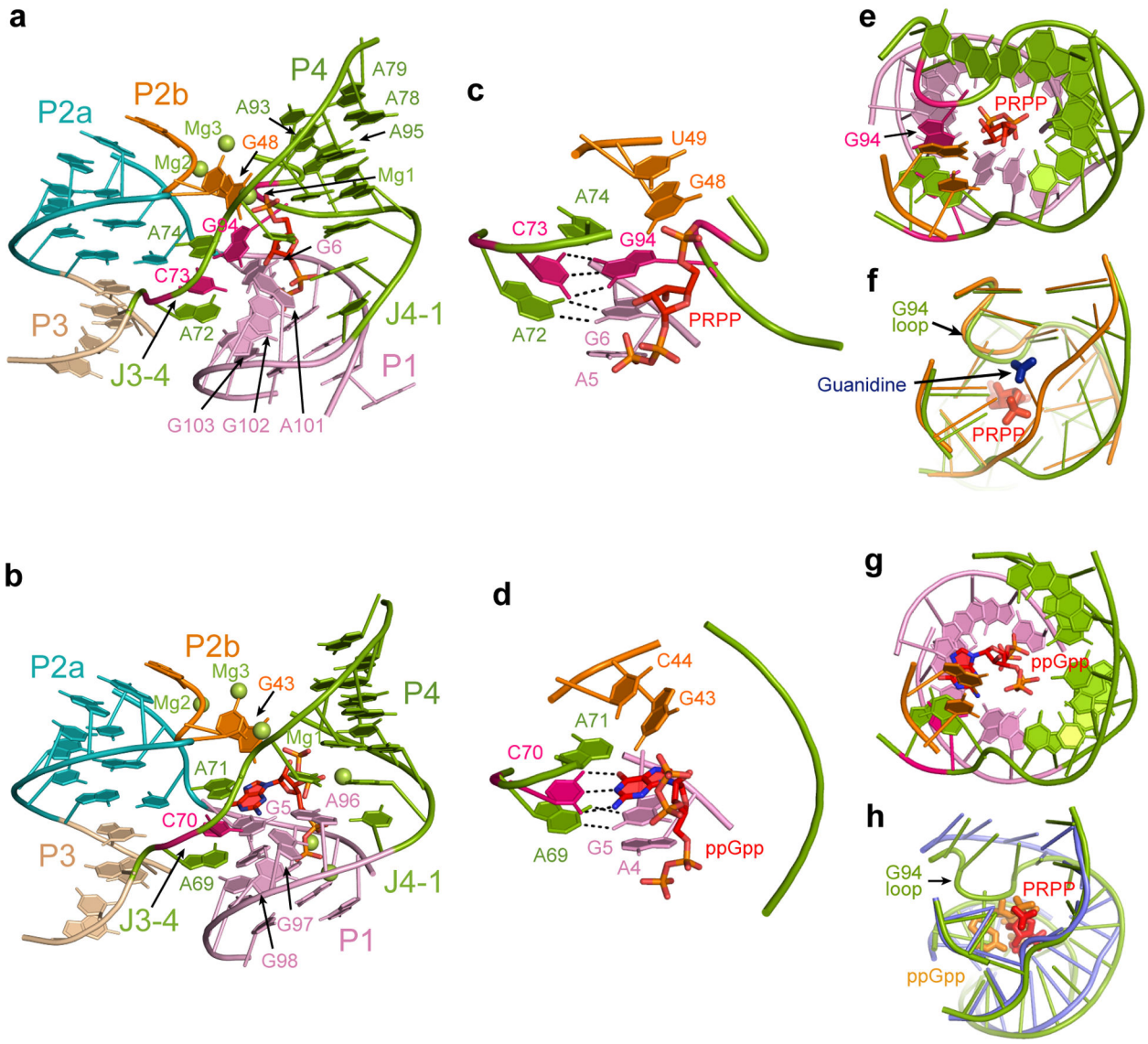

Figure 2.

Structural elements of the PRPP and ppGpp riboswitches. RNA colors correspond to the schematics in Fig. 1. Ligands are shown in atomic colors (oxygen in pink, nitrogen in blue, phosphorus in orange, carbon in red) (**a**, **b**) Zoomed-in views of the four-way junction in the PRPP (a) and ppGpp (b) riboswitches. (**c, d**) Views highlighting different recognition of the PRPP (c) and ppGpp (d) ligands. (**e**) Top view of the ligand binding tunnel in the PRPP riboswitch. (**f**) Superposition of the ligand binding pockets of the PRPP (green) and guanidine (orange) riboswitches. PRPP in red, guanidine in blue. (**g**) Top view of the ligand binding tunnel in the ppGpp riboswitch. (**h**) Superposition of the ligand binding pockets of the PRPP (green) and ppGpp (blue) riboswitches. PRPP in red, ppGpp in orange.

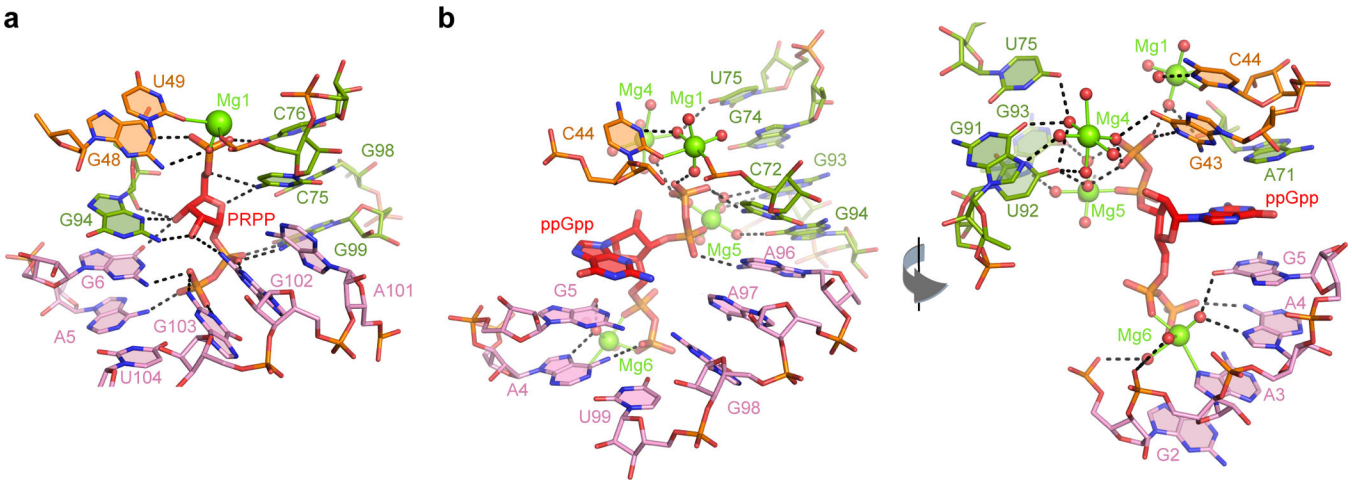

Figure 3.

Molecular details of the RNA-ligand recognition. All molecules are shown in atomic colors with putative hydrogen bonds depicted in black dashed lines. Mg^{2+} cations are shown as green spheres and their coordinating bonds are depicted in thin green sticks. Water molecules are shown as red spheres. Some residues are removed for clarity. (**a**) Recognition of PRPP by the riboswitch RNA. (**b**) Two views showing recognition of ppGpp by the riboswitch RNA.

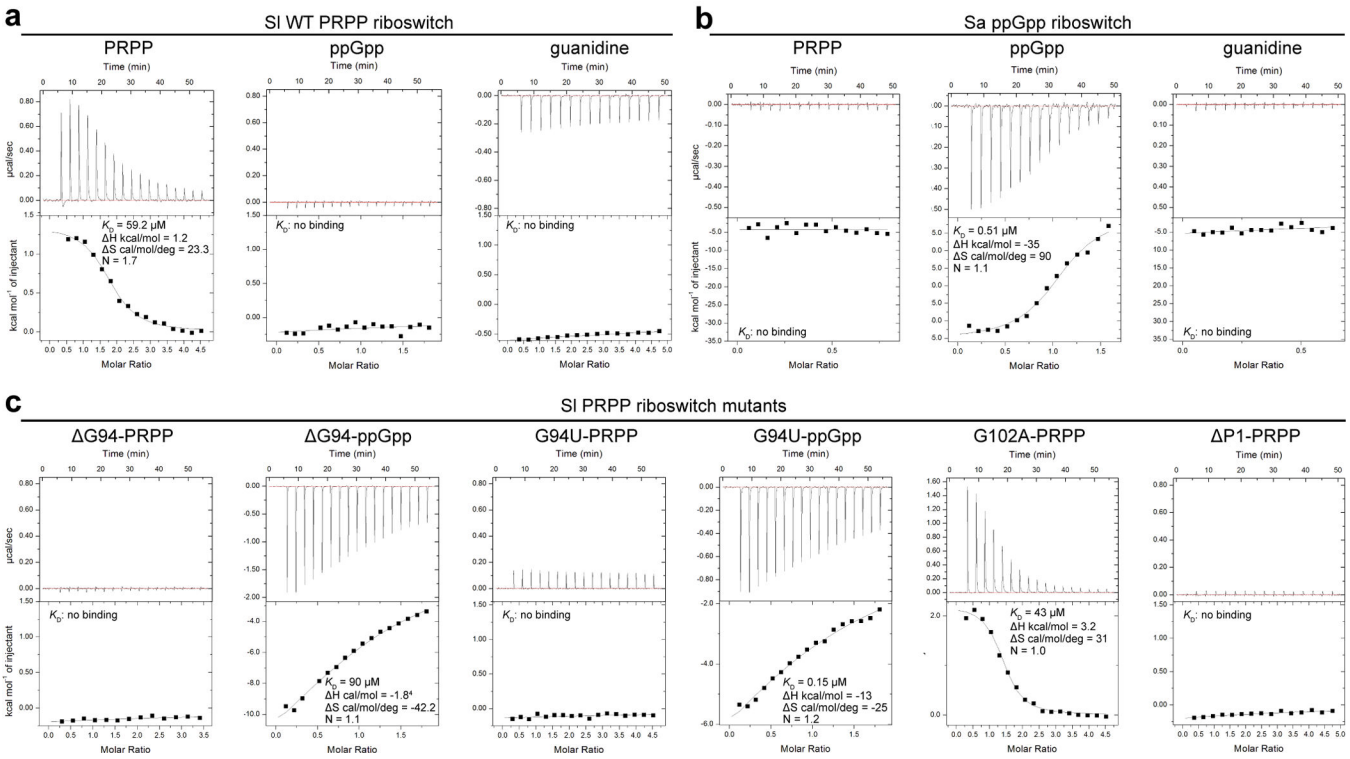

Figure 4.

Binding affinity of RNA-ligand interactions determined by ITC. K_Ds are the average of two experiments ± standard error. (**a**) Representative ITC titrations and integrated fitted heat plots for binding of the wild type (WT) *S. lipocalidus* (Sl) PRPP riboswitch RNA to various ligands. (**b**) Same as (a) for the *S. acidophilus* (Sa) ppGpp riboswitch RNA used in crystallization (WT/CC). (**c**) Same as (a) for the mutants of the *S. lipocalidus* PRPP riboswitch.

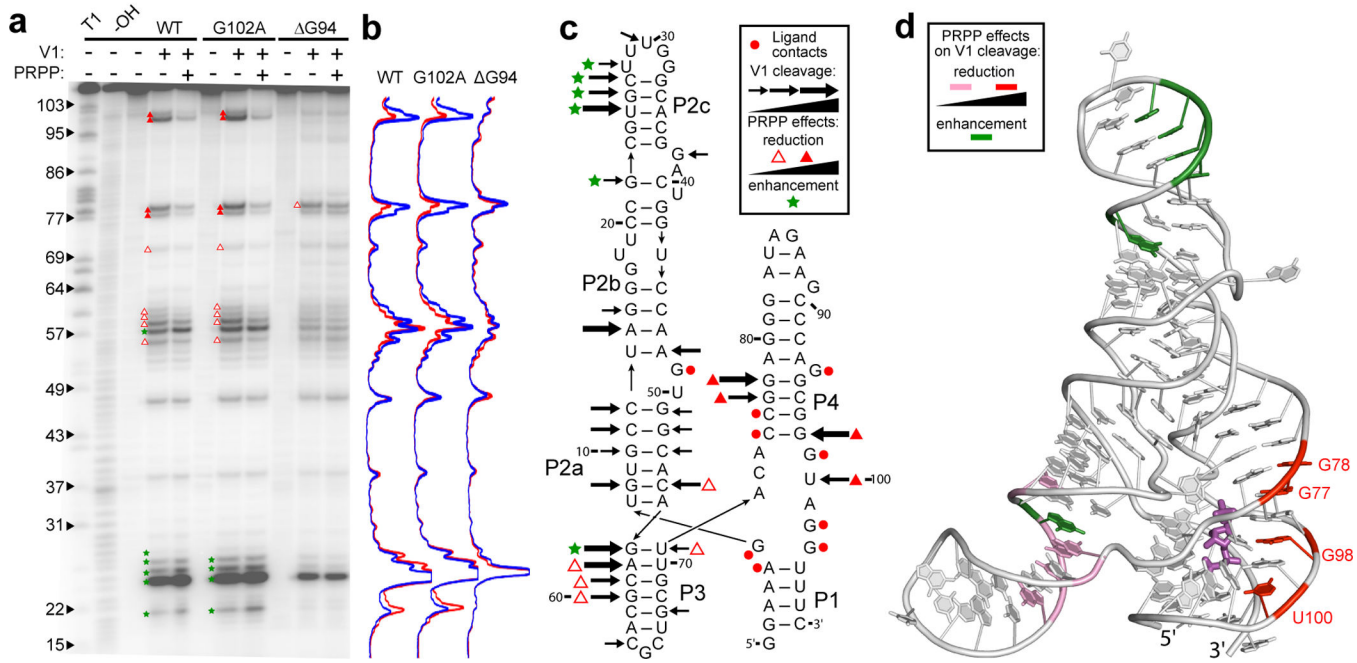

Figure 5.

Nuclease probing of the PRPP riboswitch RNA structure. (**a**) V1 nuclease cleavage of the 5′ ^{32}P-labelled 107-nt wild type (WT) and mutant RPRP riboswitch RNAs (0.5 μM) in the absence and presence of 2 mM PRPP. The cleavage was analyzed on an 8M urea/10% polyacrylamide gel. T1 and -OH designate RNase T1 and alkaline ladders, respectively. PRPP-induced effects are shown with symbols described in the inset to panel (c). (**b**) Cleavage intensity profiles of the V1-digested RNAs in the absence (blue line) and presence (red line) of PRPP, determined for each lane of the gel in panel (a). (**c**) Summary of the V1 cleavage and footprinting results. Symbols are described in the inset. Red circles show nucleotides directly involved in ligand binding. Note that PRPP-induced effects on short (<15 nt) RNAs were not captured. (**d**) Projections of the PRPP-induced effects on the riboswitch structure.

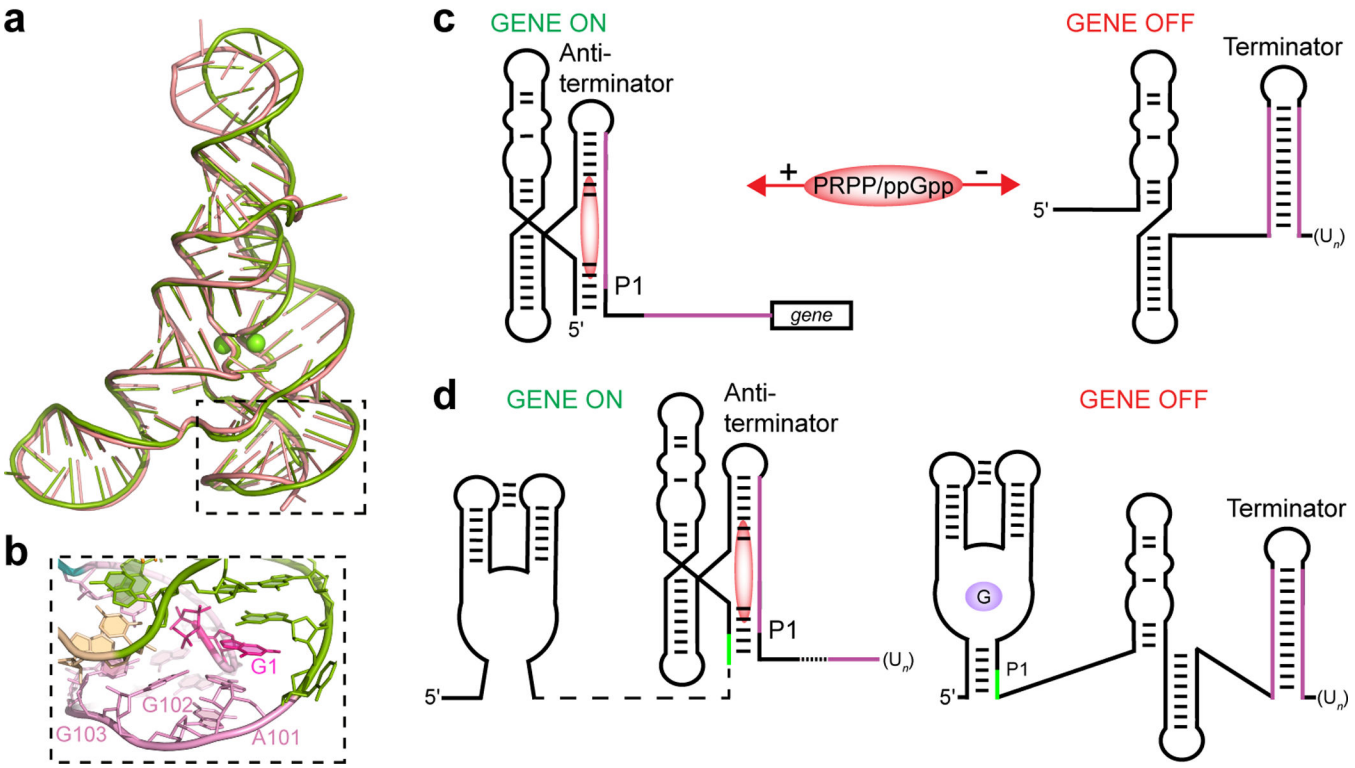

Figure 6.

Proposed mechanisms of the PRPP and ppGpp riboswitch action. (**a**) Superposition of the *apo* (green) and ligand-bound (pink) structures of the PRPP riboswitch. Arrow shows a conformational change in the *apo* structure. (**b**) Zoomed-in view of the P1 helix showing movement of G1 inside the ligand-binding tunnel. (**c**) Schematic of the transcription activation mechanism of the PRPP and ppGpp riboswitches. Two panels show mutually exclusive ligand-bound and *apo* conformations, which form either antiterminator or terminator hairpins, respectively. (**d**) Schematic highlighting two mutually exclusive guanine- and PRPP-bound conformations of the tandem guanine-PRPP riboswitch. The two sensors share a small element (green line) which can be engaged in the formation of the alternative structures.